PAPER

Efficient biodiesel production from oleic acid using metal–organic framework encapsulated Zr-doped polyoxometalate nano-hybrids

Qiuyun Zhang, [ID] *[ab] Dandan Lei,[a] Qizhi Luo,[a] Jialu Wang,[c] Taoli Deng,[a] Yutao Zhang*[bc] and Peihua Ma*[d]

According to the need of sustainable development, solid catalysts are critical materials for green biodiesel production. In this study, a hydrothermal method was used to develop a reusable and highly active Fe-BTC and UiO-66 metal–organic framework encapsulated Zr-doped polyoxometalate nano-hybrid catalysts (ZrSiW/Fe-BTC and ZrSiW/UiO-66) for the acid-catalyzed esterification of oleic acid with methanol. The structural and compositional characterization of the synthesized catalysts were characterized using various techniques such as Fourier transform infrared spectrometry (FT-IR), X-ray diffraction (XRD), nitrogen adsorption–desorption, scanning electron microscopy (SEM), and thermogravimetric (TG) and temperature programmed desorption (NH_3-TPD) analysis. The as-prepared ZrSiW/UiO-66 had excellent catalytic activity in the esterification of oleic acid with methanol, higher than that of ZrSiW/Fe-BTC catalyst, owing to the fact that ZrSiW/UiO-66 nano-hybrids have high acidity, large specific surface area and pore volumes, and relatively large average pore sizes. Furthermore, the reusability and stability of nano-hybrids were also evaluated, and it was found that the stability of ZrSiW/UiO-66 catalyst was better.

1. Introduction

Due to the inevitable future decline of fossil fuel resources, the current increasing prices of fuels, and environmental concerns, such as global warming,[1] several alternative energy sources of fossil fuels have been proposed, *e.g.* biomass, biodiesel, and solar energy, *etc.* Biodiesel (fatty acid methyl esters) is considered as a potential replacement for fossil fuels, and has some advantages, for example, biodegradability, non-toxicity, higher cetane index, and lower emissions of CO_2.[2,3] In general, the synthesis of biodiesel uses esterification or transesterification from vegetable oils, animal fats, waste cooking oils, algae, and fatty acids with methanol in the presence of a homogeneous, heterogeneous, or enzymatic catalyst.[4] However, bio-enzyme catalytic progress is still difficult due to its poor stability and the high cost of the enzyme.[5] On the contrary, homogeneous acid/base catalysts (such as NaOH, KOH, H_2SO_4, HCl) are commonly employed for the commercial production of biodiesel, but they are difficult to recycle, large amounts of

wastewater are generated, and they have high corrosiveness.[6] Accordingly, in an attempt to avoid the drawbacks of liquid acid/base catalysts, the use of heterogeneous solid catalysts is currently being investigated, due to its non-corrosive nature, and being easy to separate products, and often recyclable.[7] However, for fatty acids and raw materials that contain a high amount of free fatty acids, heterogeneous base catalysts react with the fatty acids to form soaps leading to low product quality.[8] In such cases, heterogeneous solid acid catalyst is preferable, because it can avoid saponification.

Various types of heterogeneous acid catalysts, such as solid superacids,[9] Cr–Al oxides,[10] SLO/HZSM-5 zeolites,[11] cation-exchange resins,[12] Fe_3O_4@HKUST-1-ABILs,[13] magnetic Fe_3O_4/MCM-41,[14] and carbon-based solid acids[15] have been applied to catalytic esterification for produce biodiesel. Unfortunately, these reported catalytic systems show one or more of the following disadvantages such as high cost, lower conversion, and catalyst toxicity. Previous studies showed that heteropolyacids are high active acidic catalysts for organic reactions,[16,17] but pure heteropolyacids are freely soluble in polar media that make their recovery difficult, as well low surface area.[18,19] To circumvent these penalties, heteropolyacids encapsulation into porous supports was attempted to heterogenize heteropolyacids.[20,21]

In recent years, metal organic frameworks (MOFs) are considered as a supported owing to possess advantageous properties, such as structural diversity, tenability, porosity, and high surface area.[22,23] Hence it was of interest to investigate the

[a] *School of Chemistry and Chemical Engineering, Anshun University, Anshun, 561000, Guizhou, China. E-mail: qyzhang.asu@gmail.com*

[b] *Engineering Technology Center of Control and Remediation of Soil Contamination of Provincial Science & Technology Bureau, Anshun University, Anshun, 561000, Guizhou, China. E-mail: zyt0516@126.com*

[c] *School of Resource and Environmental Engineering, Anshun University, Anshun, 561000, Guizhou, China*

[d] *School of Chemistry and Chemical Engineering, Guizhou University, Guiyang, 550025, Guizhou, China. E-mail: phma@gzu.edu.cn*

heteropolyacids anchored to MOFs catalyst for biodiesel production. In this work, Zr-doped silicotungstic acid supported on MOFs (Fe-BTC and UiO-66) were synthesized and characterized and their catalytic performances for the esterification of oleic acid with methanol were evaluated. The experimental conditions, such as reaction temperature and time, the molar ratio of oleic acid to methanol, and the amount of catalyst, were optimized. Finally, the reusability of the synthesized catalysts was also investigated.

2. Experimental

2.1 Materials

All chemicals were of analytical grade and used as received without further purification. Zirconium(IV) oxynitrate hydrate (AR), iron(III) nitrate nonahydrate ($Fe(NO_3)_3 \cdot 9H_2O$, AR), N,N-dimethylformamide (DMF, AR), oleic acid (AR), absolute ethanol (AR), and anhydrous methanol (AR) were purchased from Sinopharm Chemical Regent Co., Ltd. Zirconium(IV) chloride, 1,3,5-benzene tricarboxylic acid (H_3-BTC, AR), terephthalic acid (AR) and silicotungstic acid (HSiW, $H_4SiW_{12}O_{40} \cdot nH_2O$, AR) were purchased from Shanghai Aladdin Industrial Inc.

2.2 Synthesis of MOFs encapsulated Zr-doped HSiW nano-hybrids

For the preparation of Zr-doped HSiW salts (ZrSiW),[24] 0.57 g of HSiW was dissolved in distilled water, and the solution of zirconium nitrate was then added dropwise into the above solution. The mixture was stirred at room temperature for 1 h and then treated at 70 °C for 3 h, the obtained ZrSiW materials were dried overnight at 110 °C.

ZrSiW/UiO-66 nano-hybrids was synthesized previously our reported method.[25] Briefly, 0.51 g of $ZrCl_4$ and 0.3275 g of terephthalic acid were dissolved in 18 mL DMF solution. Then, the above-prepared ZrSiW salts was added to the above solutions with stirring at room temperature for 1 h. The obtained mixture was put in a 50 mL Teflon-lined stainless-steel autoclave and heated oven at 120 °C for 6 h. After cooling down to room temperature, the solid was separated by centrifugation, and washed with DMF for three times and distilled water for three times. The product was finally dried in an oven at 120 °C for 24 h. By comparison, UiO-66 sample without ZrSiW was also synthesized the use of the same method.

ZrSiW/Fe-BTC nano-hybrids was synthesized by 2.42 g of iron(III) nitrate nonahydrate and the above-prepared ZrSiW salts were dissolved in 18 mL distilled water. Then, 0.63 g of H_3-BTC was added to the above solutions with stirring at room temperature for 1 h. The obtained mixture was put in a 50 mL Teflon-lined stainless-steel autoclave and heated oven at 120 °C for 6 h. After cooling down to room temperature, the solid was separated by centrifugation, and washed with 150 mL of ethanol for three times. Subsequently, the powder was treated with hot ethanol for 3 h several times. The product was finally dried in an oven at 120 °C for 24 h. By comparison, Fe-BTC sample without ZrSiW was also synthesized the use of the same method.

2.3 Material characterization

Fourier-transformed infrared spectroscopy (FTIR) spectra of synthesized catalysts were recorded on KBr pellets using a PerkinElmer spectrum 100 in the range of 400–4000 cm^{-1}. Wide-angle X-ray diffraction (XRD) patterns were recorded on a D8 ADVANCE (Germany) using CuKα (1.5406 Å) radiation to determine the structure of synthesized nano-hybrids. The morphology of the nano-hybrids was determined by a scanning electron microscope (SEM) at 2.0 kV (Hitachi S4800). The pore structure of the nano-hybrids was analyzed by nitrogen adsorption–desorption isotherms with a quantachrome instrument (Quantachrome Instruments, Boynton Beach, USA). Thermogravimetric (TG) analysis was carried out in a NETZSCH/STA 409 PC Luxx simultaneous thermal analyzer, the samples were heated up from room temperature to 600 °C, at a heating rate of 5 °C min^{-1}. The acidic properties of the nano-hybrids was characterized by temperature programmed desorption (NH_3-TPD) (Micromeritics AutoChem II 2920).

2.4 Catalytic activity

Typically, the esterification reactions of oleic acid with methanol were performed in a 50 mL stainless steel reactor equipped with a magnetic stirrer, the required amount nano-hybrids catalyst was also added. Subsequently, the reaction system was stirred and heated to the specified temperature in an oil bath. Following each run, the reactor was cooled down to room temperature, the catalyst was separated by centrifugation, and the reaction mixture was moved into a rotary evaporator to remove excess methanol and water. The conversion of the esterification reaction was determined by the initial of acid value in the mixture and the final of acid value, and the acid value was estimated according to the ISO 660-2009 standard method.

3. Results and discussion

3.1 Catalysts characterization

3.1.1 FTIR analysis. The preparation of catalysts was analyzed by FTIR spectra, as shown in Fig. 1a and b. FT-IR spectra of ZrSiW have characteristic bands of Keggin's structure of HSiW at 980 (W=O), 927 (Si–O), 884 (W–O_c–W), and 781 (W–O_e–W) cm^{-1}.[26] In addition, the four typical peaks also were observed with some shift from ZrSiW/Fe-BTC and ZrSiW/UiO-66 nano-hybrids, this is probably due to the robust interaction between the Keggin unit and framework structure owing to the strong adsorption at the interface,[27] determining the ZrSiW molecules were embedded on MOFs matrix. Compared with Fe-BTC, the same absorption peaks (1636, 1585, 1454, 759, and 710 cm^{-1}) of ZrSiW/Fe-BTC catalyst also was observed and related to the Fe-BTC framework structure.[28] A similar phenomenon was found between UiO-66 and ZrSiW/UiO-66. It should be noted that the above results provide evidence of the encapsulation of ZrSiW into MOFs materials.

3.1.2 XRD analysis. The XRD patterns of ZrSiW, Fe-BTC, ZrSiW/Fe-BTC, UiO-66, and ZrSiW/UiO-66 are given in Fig. 2a and b. It is clear that the heteropoly acid salt ZrSiW is relatively
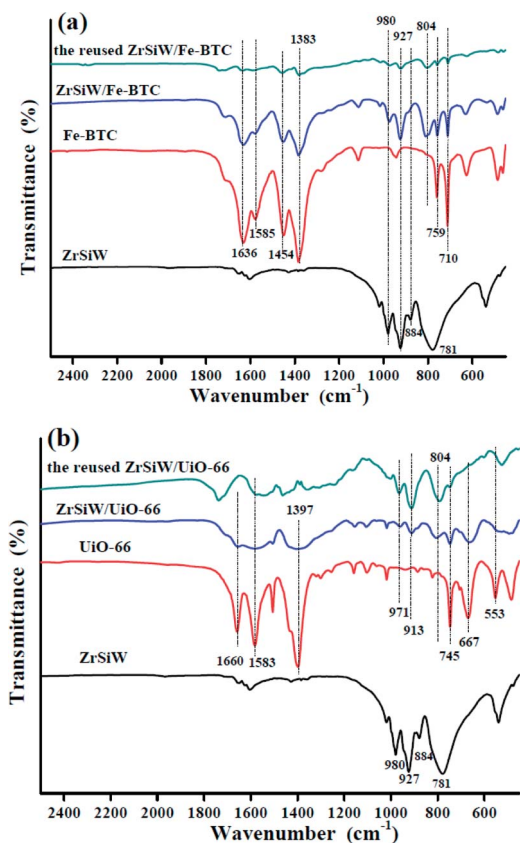
Fig. 1 FTIR spectra of ZrSiW, Fe-BTC, ZrSiW/Fe-BTC, and ZrSiW/Fe-BTC after sixth run (a); FTIR spectra of ZrSiW, UiO-66, ZrSiW/UiO-66, and ZrSiW/UiO-66 after sixth run (b).
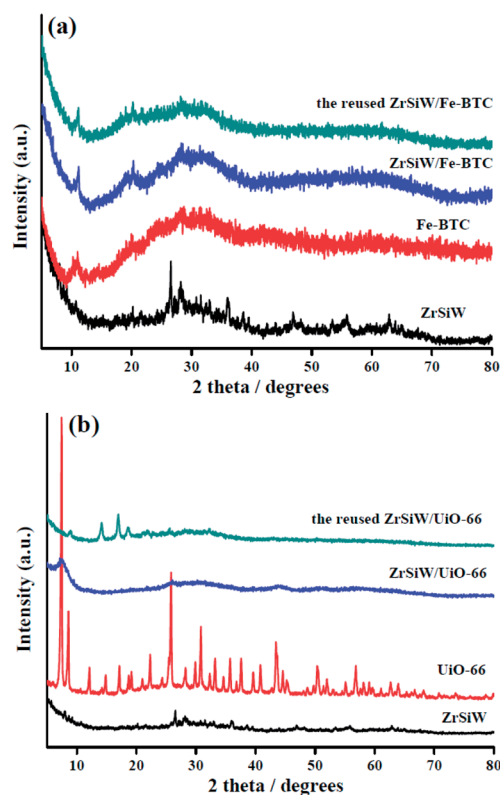

Fig. 2 The XRD patterns of ZrSiW, Fe-BTC, ZrSiW/Fe-BTC, and ZrSiW/Fe-BTC after sixth run (a); the XRD patterns of ZrSiW, UiO-66, ZrSiW/UiO-66, and ZrSiW/UiO-66 after sixth run (b).

high crystalline, whereas Fe-BTC is less crystalline and UiO-66 is highly crystalline, which is probably due to the use of the different organic ligand. When the ZrSiW was embedded in MOFs matrix, a complete disappearance of peaks at 25.7° and 28.2° assigned to ZrSiW crystalline was observed from ZrSiW/Fe-BTC and ZrSiW/UiO-66 nano-hybrids, indicating that proper encapsulation of ZrSiW into the Fe-BTC and UiO-66 material. The results are in agreement with the reported similar studies in the literature.[29] Remarkably, the ZrSiW/UiO-66 nano-hybrids reveals a broad peak and predominatingly contains an amorphous state, this result might be attributed to that the interaction between Zr-doped polyoxometalates species and the MOFs materials. Similar results could also be observed from our previous studies.[30] These characterization results mentioned above again suggests the preparation of the catalyst is successful.

3.1.3 Nitrogen adsorption–desorption analysis. The nitrogen adsorption–desorption hysteresis and pore size distribution plots of the ZrSiW/Fe-BTC and ZrSiW/UiO-66 nano-hybrids are depicted in Fig. 3a and b. As can be revealed, the nitrogen adsorption/desorption isotherms of ZrSiW/Fe-BTC is between types I and IV shapes with a hysteresis loop. Accordingly, the ZrSiW/Fe-BTC catalyst can be classified as micro- and mesopores material. For comparison, nitrogen isotherms of ZrSiW/UiO-66 catalyst reveal a type-IV shape pattern with a H4 hysteresis loop in the range of 0.50–0.97 relative pressure, which

suggests that mesopores exist. As expected, the average pore diameter, pore volume and surface area of ZrSiW/UiO-66 (3.9 nm, 0.243 m^3 g^{-1}, and 249.4 m^2 g^{-1}) are higher than the ZrSiW/Fe-BTC sample (2.8 nm, 0.135 m^3 g^{-1}, and 191.5 m^2 g^{-1}). These data suggest that the relatively large pores and high surface area of ZrSiW/UiO-66 hybrids are beneficial to the formation of active sites, providing excellent catalytic activity for the synthesis of biodiesel.

3.1.4 SEM analysis of the catalysts. The surface structure of the synthesized materials was analyzed by SEM (Fig. 4). SEM image of ZrSiW salts shown in Fig. 4a provides big block morphology. When the ZrSiW was embedded in MOFs cages, by comparing two images (Fig. 4b and c), the micrographs of Fe-BTC and ZrSiW/Fe-BTC are similar to each other, and it is a nearly spherical irregular morphology with diameter of ~200 to 300 nm. For UiO-66 and ZrSiW/UiO-66, the micrographs of UiO-66 was also near-spherical irregular and aggregated shapes with an average size of nearly 200 nm. In contrast, the addition of ZrSiW by hydrothermal method has no significant effect on the near-spherical structure of UiO-66, and the resulting ZrSiW/UiO-66 particles are good dispersion and their particles size is in the range of 50–200 nm. It suggests that the encapsulation of ZrSiW into UiO-66 prevents the aggregation of UiO-66 particles. All the results show that the Fe-BTC and UiO-66 have a strong stability.

3.1.5 TG analysis. In this study, TG analysis was used in analyzing the thermal stability of the nano-hybrids catalysts, and the graphs revealed the weight loss (Fig. 5). For the ZrSiW
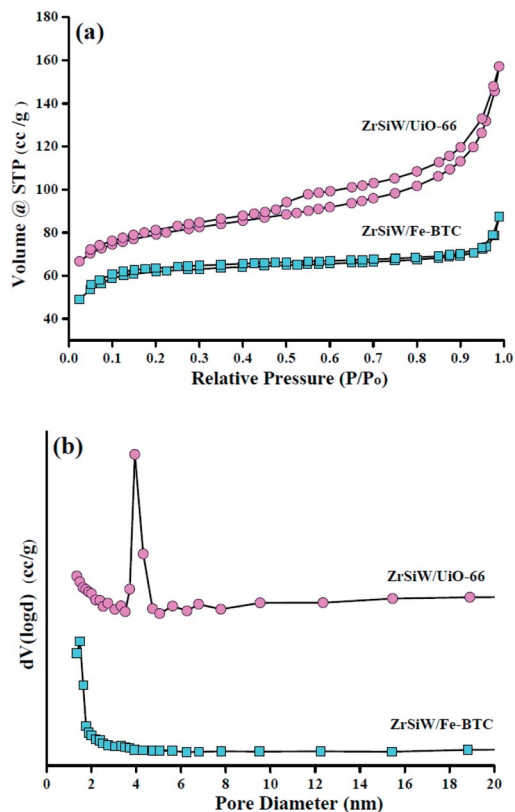
Fig. 3 Nitrogen adsorption–desorption isotherm plot of ZrSiW/Fe-BTC and ZrSiW/UiO-66 hybrids (a); pore size distribution of ZrSiW/Fe-BTC and ZrSiW/UiO-66 hybrids (b).
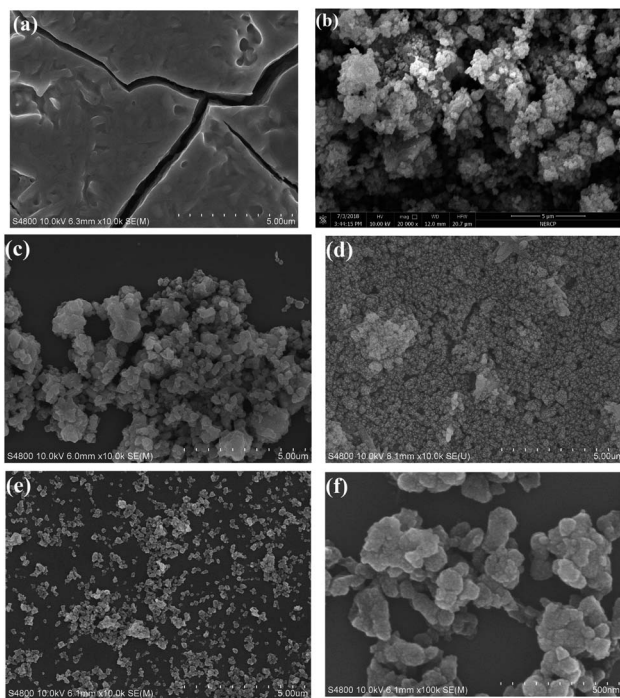

Fig. 4 SEM images of resultant materials: (a) ZrSiW, (b) Fe-BTC, (c) ZrSiW/Fe-BTC, (d) UiO-66, (e and f) ZrSiW/UiO-66 materials.
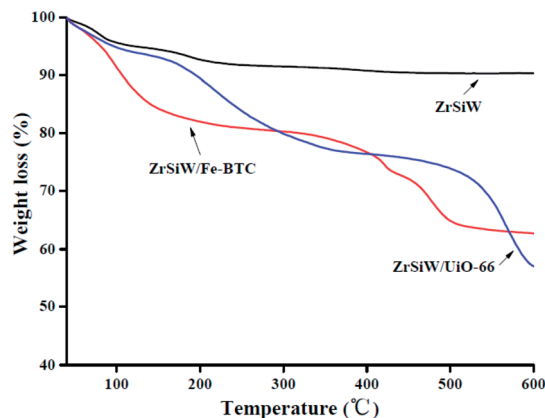

Fig. 5 TG analysis of ZrSiW, ZrSiW/Fe-BTC and ZrSiW/UiO-66 hybrids.

sample, it exhibits a weight loss from 40 to 600 °C and the weight loss of about 10% is depicted to the loss of physically adsorbed water molecules and strongly adsorbed water molecules present in the catalyst. For comparison, the two nano-hybrids, the weight loss values of 20% from 40 to 300 °C is mainly due to the loss of water molecules and solvent, and the weight loss of about 20% from 300 to 600 °C can be assigned to the decomposition of the organic ligand and the destruction of the metal–organic framework.[31] Based on the figure, the ZrSiW/ UiO-66 nano-hybrids show relatively higher thermal stability compared to ZrSiW/Fe-BTC catalyst as the main decomposition of the organic ligand started at higher temperature, which is between 500 and 600 °C compared to ZrSiW/Fe-BTC catalyst that started at 400 °C that indicates the high stability of UiO-66, similar to the result observed in SEM. The data of TG suggests that the prepared nano-hybrids have excellent thermal stability in the experiments.

3.1.6 NH$_3$-TPD analysis. The TPD analysis of ZrSiW/Fe-BTC and ZrSiW/UiO-66 nano-hybrids using NH$_3$ as probe gases are shown in Fig. 6. In general, the peak temperature and area the curves can be used to calculate the acid strength and the relative concentration of the acid.[32] For two nano-hybrids, a smaller broad NH$_3$ desorption peak was formed at 100–150 °C, which indicating that the two nano-hybrids had weak acid sites. Surprisingly, as for ZrSiW/UiO-66 nano-hybrids, another NH$_3$ desorption peak appeared at 150–300 °C, and the ZrSiW/UiO-66 nano-hybrids total acidity was found to be 18 mmol g^{-1}, suggesting the sample had medium acid sites. By contrast, no absorption peak of the ZrSiW/Fe-BTC nano-hybrids was appeared at 150–300 °C. From the NH$_3$-TPD result shows the acidity of ZrSiW/UiO-66 is higher than that of ZrSiW/Fe-BTC, which is main advantages for catalytic esterification reactions.

3.2 Effect of esterification conditions

Esterification reaction of oleic acid with methanol was conducted in the presence of ZrSiW/Fe-BTC and ZrSiW/UiO-66 nano-hybrids catalyst to determine the catalytic activity in the production of biodiesel. Thus, in this work, the effect of different reaction parameters on the conversion of methyl
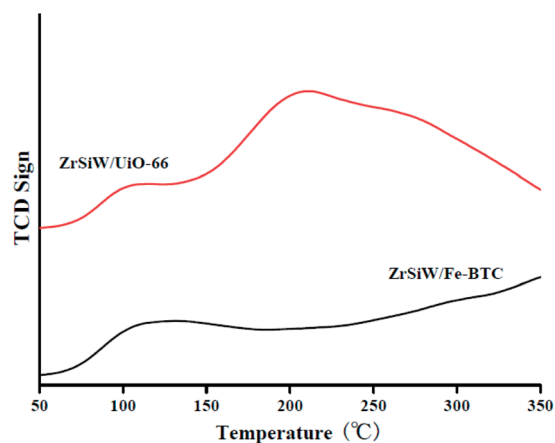
Fig. 6 Acidity of ZrSiW/Fe-BTC and ZrSiW/UiO-66 hybrids as measured by TPD of NH_3.

oleate was investigated. The parameters were oleic acid/methanol molar ratio, temperature, time, and catalyst loading. The optimum conditions for the esterification reaction were performed and the results are shown in Fig. 7 and 8.

3.2.1 Effect of reaction time and temperature. The influence of reaction time as a process parameter for the production of methyl oleate was also investigated with a catalyst loading of 0.24 g and the oleic acid/methanol molar ratio of 1 : 20 at 150 °C. The results, as shown in Fig. 7a indicated that the oleic
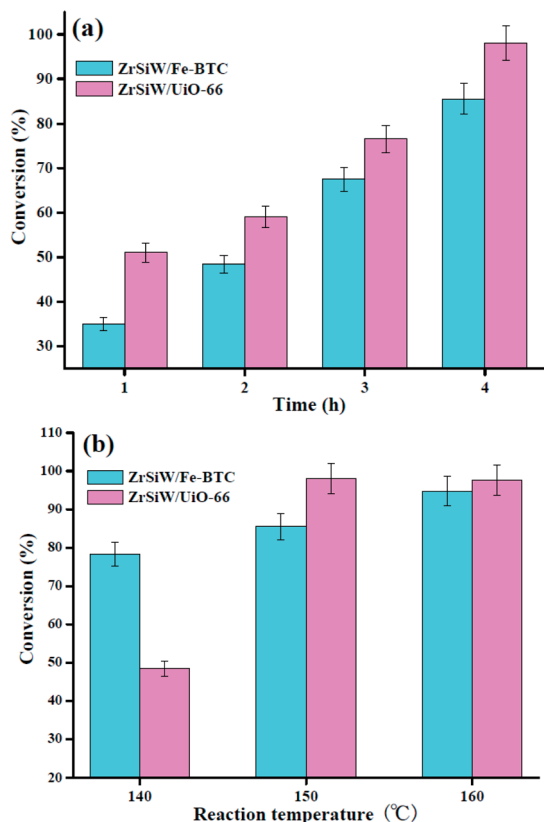

Fig. 7 Effect of reaction time (a) and temperature (b) on the esterification.
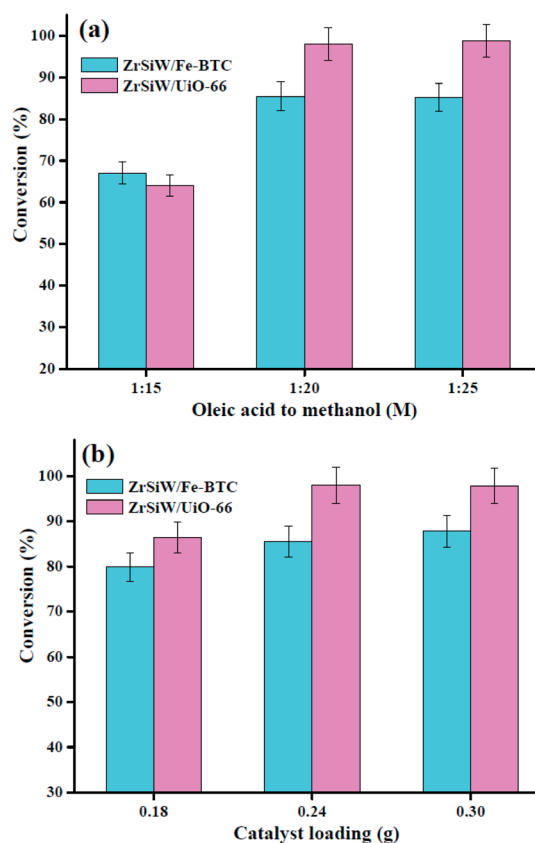

Fig. 8 Effect of molar ratio of oleic acid to methanol (a) and catalyst loading (b).

acid conversion was improved with the increase in the time. When the time rose to 4 h, the oleic acid conversion increased to 85.5% and 98.0% for ZrSiW/Fe-BTC and ZrSiW/UiO-66 nano-hybrids, respectively, and reached at its maximum, and a similar reaction condition was presented by Nandiwale *et al.*[33] Interestingly, the activity of ZrSiW/UiO-66 was much better than ZrSiW/Fe-BTC catalyst, and these significant results may be associated with the ZrSiW/UiO-66 nano-hybrids possess highly acidic. Finally, in present study, 4 h reaction time is sufficient for the esterification of oleic acid with methanol.

To study the effect of the reaction temperature on the conversion of biodiesel, some experiments were carried out using ZrSiW/Fe-BTC and ZrSiW/UiO-66 nano-hybrids at 140, 150, and 160 °C with a catalyst loading of 0.24 g and the oleic acid/methanol molar ratio of 1 : 20 at 4 h (Fig. 7b). The results showed that the conversion rate is accelerated at a higher temperature, and reached an optimum conversion of 98.0% for ZrSiW/UiO-66 catalyst at the temperature of 150 °C. At the temperature higher than 150 °C, the oleic acid conversion started to increase slowly. In similar work performed by Araujo *et al.*[34] Hence, 150 °C was choose as the optimum reaction temperature.

3.2.2 Effect of molar ratio and catalyst loading. In the next step, the effect of oleic acid/methanol molar ratio was examined by using these nano-hybrids with a catalyst loading of 0.24 g at 150 °C for 4 h reaction times was examined. The oleic acid/
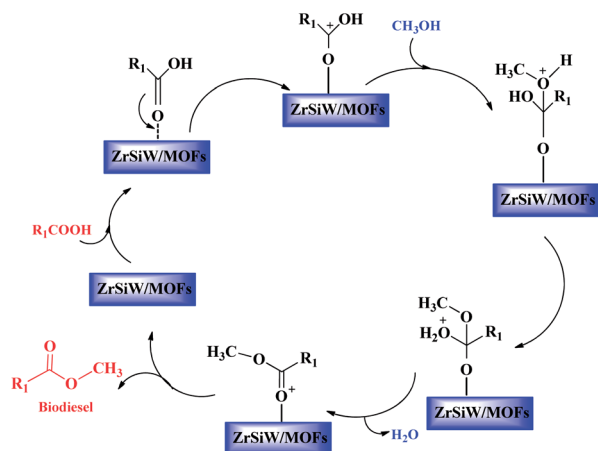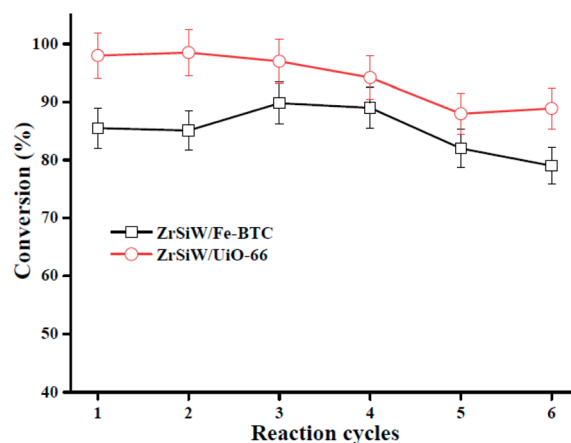
Fig. 9 Possible mechanism of esterification.

Fig. 10 Reusability study. Reaction conditions: oleic acid/methanol molar ratio 1 : 20, reaction temperature 150 °C, catalyst loading 0.24 g, reaction time 4 h.

methanol molar ratio varied from 1 : 15 to 1 : 25, and the results are depicted in Fig. 8a. When the oleic acid/methanol molar ratio is 1 : 15, the oleic acid conversion is low. However, the oleic acid conversion is obtained with a molar ratio of oleic acid to methanol 1 : 20 about 85.5% and 98.0% for ZrSiW/Fe-BTC and ZrSiW/UiO-66 nano-hybrids, respectively. Subsequently, further increase in molar ratio to 1 : 25, the oleic acid conversion remains almost constant probably because of mass transfer limitation caused by dilution. Therefore, in present study, molar ratio of oleic acid to methanol 1 : 20 was chosen as the optimum ratio.

Subsequently, the effect of the catalyst loading on the oleic acid esterification reaction was assessed under optimum reaction conditions: the oleic acid/methanol molar ratio of 1 : 20 at 150 °C for 4 h. From Fig. 8b, a closer look at the results reveals with the increase in the catalyst loading from 0.18 g to 0.24 g, the conversion increased from 79.9% to 85.5% for ZrSiW/Fe-BTC nano-hybrids, and the conversion increased from 86.4% to 98.0% for ZrSiW/UiO-66 nano-hybrids. However, when a catalyst loading of 0.30 g was used, a conversion of 87.8% and 97.9% was reached for ZrSiW/Fe-BTC and ZrSiW/UiO-66 nano-hybrids, respectively, remaining practically constant. Further increase in catalyst loading probably decreased the conversion due to the agglomeration of nano-hybrids, poor diffusion of reactants and products.[35] Thus, optimum catalyst loading in this study for biodiesel synthesis is 0.24 g.

3.3 Plausible mechanism for esterification

Fig. 9 displays a plausible mechanism for esterification reactions. In general, carbonyl group of fatty acids is adsorbed on the nano-hybrids catalyst to form the protonated carbonyl group, following alcohol molecule attacked the protonated carbonyl group in the liquid phase, and finally the water molecules was removed to produce an ester.[36–39]

3.4 Reusability of catalyst

As mentioned above, we focus on ZrSiW/Fe-BTC and ZrSiW/UiO-66 nano-hybrids catalysts with recyclability in the present work.

After each catalytic cycle, the catalysts (ZrSiW/Fe-BTC as well as ZrSiW/UiO-66) was recovered by centrifugation, washed by methanol (two times), and directly use in the next cycle. Thus, the reusability of two nanocatalysts was evaluated for six cycles (Fig. 10). For two nano-hybrids, the catalytic activity was retained in three successive cycles. However, the catalytic activity slightly decreased so that at sixth cycle the oleic acid conversion was 79% and 88.9% for ZrSiW/Fe-BTC and ZrSiW/UiO-66 nano-hybrids, respectively. In order to investigate the activity of slightly deactivation, FTIR and XRD analysis were used to determine the catalyst stability (see Fig. 1 and 2). Based on the characterization results, the XRD and FTIR spectra of the sixth recovery catalyst is similar with the fresh, suggesting the better recyclability of two nano-hybrids. This may be attributed to the strong interaction between ZrSiW molecules and MOFs enhanced their stabilities in esterification reaction. Moreover, the catalytic activity still decreases slightly mainly because of leaching part of active component during repeated reactions. In comparison with earlier reported solid acid nanocatalyst,[40,41] the synthesized nano-hybrids showed greater stability for biodiesel synthesis.

4. Conclusions

ZrSiW/Fe-BTC and ZrSiW/UiO-66 nano-hybrids were prepared by a hydrothermal process. The nano-hybrids are suitable for the catalytic esterification of oleic acid with methanol. The ZrSiW/UiO-66 nano-hybrids exhibits remarkable catalytic activity in contrast to ZrSiW/Fe-BTC. Characterization analyses indicated that the ZrSiW/UiO-66 possess an appropriate structure and high acidity. The highest oleic acid conversion of 98.0% was obtained using the ZrSiW/UiO-66 nano-hybrids nanocatalyst under the optimal esterification reactions: 150 °C, 0.24 g catalyst, 1 : 20 molar ratio of oleic acid to methanol and a reaction time of 4 h. Moreover, the ZrSiW/UiO-66 nano-hybrids could be easily recovered by centrifugation, and reused for six consecutive runs without substantial losses of

activity. The present work provides an inexpensive and environmentally friendly method to synthesize metal–organic frameworks embedded Zr-doped polyoxometalates nanohybrids and may contribute to the economical benefits of biodiesel synthesis.

Conflicts of interest

There are no conflicts to declare.

Acknowledgements

Notes and references

1 C. Poonjarernsilp, N. Sano, N. Sawangpanich, T. Charinpanitkul and H. Tamon, *Green Chem.*, 2014, **16**, 4936–4943.

2 L. T. Wang, X. Q. Dong, H. X. Jiang, G. M. Li and M. H. Zhang, *Fuel Process. Technol.*, 2014, **128**, 10–16.

3 I. Ambat, V. Srivastava and M. Sillanpää, *Renewable Sustainable Energy Rev.*, 2018, **90**, 356–369.

4 Q. Y. Zhang, F. F. Wei, P. H. Ma, Y. T. Zhang, F. H. Wei and H. L. Chen, *Waste Biomass Valorization*, 2018, **9**, 911–918.

5 L. Soler, A. Illanes and L. Wilson, *Catal. Today*, 2015, **259**, 177–182.

6 Y. Chang, C. Lee and C. Bae, *RSC Adv.*, 2014, **4**, 47448–47454.

7 W. L. Xie and H. Wang, *Renewable Energy*, 2020, **145**, 1709–1719.

8 N. Sun, M. H. Zhang, X. Q. Dong and L. T. Wang, *RSC Adv.*, 2019, **9**, 15941–15948.

9 N. A. Negm, G. H. Sayed, O. I. Habib, F. Z. Yehia and E. A. Mohamed, *J. Mol. Liq.*, 2017, **237**, 38–45.

10 A. Guldhe, C. V. R. Moura, P. Singh, I. Rawat, E. M. Moura, Y. Sharma and F. Bux, *Renewable Energy*, 2017, **105**, 175–182.

11 S. S. Vieira, Z. M. Magriotis, N. A. V. Santos, A. A. Saczk, C. E. Hori and P. A. Arroyo, *Bioresour. Technol.*, 2013, **133**, 248–255.

12 J. Fu, Z. Li, S. Xing, Z. Wang, C. Miao, P. Lv and Z. Yuan, *Fuel*, 2016, **181**, 1058–1065.

13 W. L. Xie and F. Wan, *Fuel*, 2018, **220**, 248–256.

14 W. L. Xie, Y. X. Han and H. Y. Wang, *Renewable Energy*, 2018, **125**, 675–681.

15 I. F. Nata, M. D. Putra, C. Irawan and C. K. Lee, *J. Environ. Chem. Eng.*, 2017, **5**, 2171–2175.

16 Z. Sun, X. X. Duan, J. Zhao, X. H. Wang and Z. J. Jiang, *Biomass Bioenergy*, 2015, **76**, 31–42.

17 P. P. Zhao, Y. Y. Zhang, Y. Wang, H. Y. Cui, F. Song, X. Y. Sun and L. P. Zhang, *Green Chem.*, 2018, **20**, 1551–1559.

18 G. R. Bertolini, L. R. Pizzio, A. Kubacka, M. J. Munoz-Batista and M. Fernandez-Garcia, *Appl. Catal., B*, 2018, **225**, 100–109.

19 A. Kuvayskaya, S. Garcia, R. Mohseni and A. Vasiliev, *Catal. Lett.*, 2019, **149**, 1983–1990.

20 R. S. Malkar and G. D. Yadav, *Appl. Catal., A*, 2018, **560**, 54–65.

21 W. L. Xie and F. Wan, *Chem. Eng. J.*, 2019, **365**, 40–50.

22 L. Jiao, Y. Wang, H. L. Jiang and Q. Xu, *Adv. Mater.*, 2018, **30**, 1703663.

23 Y. S. Kang, Y. Lu, K. Chen, Y. Zhao, P. Wang and W. Y. Sun, *Coord. Chem. Rev.*, 2019, **378**, 262–280.

24 Q. Y. Zhang, F. F. Wei, Q. Li, J. S. Huang, Y. M. Feng and Y. T. Zhang, *RSC Adv.*, 2017, **7**, 51090–51095.

25 Q. Y. Zhang, T. T. Yang, X. F. Liu, C. Y. Yue, L. F. Ao, T. L. Deng and Y. T. Zhang, *RSC Adv.*, 2019, **9**, 16357–16365.

26 M. J. da Silva, L. C. de Andrade Leles, S. O. Ferreira, R. C. da Silva, V. K. Viveiros, D. M. Chaves and P. F. Pinheiro, *ChemistrySelect*, 2019, **4**, 7665–7672.

27 X. Liao, Y. Huang, Y. Zhou, H. Liu and Y. Cai, *Appl. Surf. Sci.*, 2019, **484**, 917–924.

28 Y. J. Yang, Y. Bai, F. Q. Zhao, E. G. Yao, J. H. Yi, C. L. Xuan and S. P. Chen, *RSC Adv.*, 2016, **6**, 67308–67314.

29 G. Ferey, C. Mellot-Draznieks, C. Serre, F. Millange, J. Dutour, S. Surble and I. Margiolaki, *Science*, 2005, **309**, 2040–2042.

30 Q. Y. Zhang, D. Ling, D. D. Lei, T. L. Deng, Y. T. Zhang and P. H. Ma, *Green Process. Synth.*, 2020, **9**, 131–138.

31 M. Zhang, Q. G. Shang, Y. Q. Wan, Q. R. Cheng, G. Y. Liao and Z. Q. Pan, *Appl. Catal., B*, 2019, **241**, 149–158.

32 S. I. Akinfalabi, U. Rashid, T. Y. C. Shean, I. A. Nehdi, H. M. Sbihi and M. M. Gewik, *Catalysts*, 2019, **9**, 482.

33 K. Y. Nandiwale and V. V. Bokade, *Ind. Eng. Chem. Res.*, 2014, **53**, 18690–18698.

34 R. O. Araujo, J. da Silva Chaar, L. S. Queiroz, G. N. da Rocha Filho, C. E. F. da Costa, G. C. T. da Silva, R. Landers, M. J. F. Costa, A. A. S. Gonçalves and L. K. C. de Souza, *Energy Convers. Manage.*, 2019, **196**, 821–830.

35 E. Viola, A. Blasi, V. Valerio, I. Guidi, F. Zimbardi, G. Broccio and G. Giordano, *Catal. Today*, 2012, **179**, 185–190.

36 J. A. Melero, J. Iglesias and G. Morales, *Green Chem.*, 2009, **11**, 1285–1308.

37 V. M. Mello, G. P. Pousa, M. S. Pereira, I. M. Dias and P. A. Suarez, *Fuel Process. Technol.*, 2011, **92**, 53–57.

38 Q. Y. Zhang, Y. T. Zhang, T. L. Deng, F. F. Wei, J. X. Jin and P. H. Ma, *Biomass, Biofuels, Biochemicals: Recent Advances in Development of Platform Chemicals*, 2020, pp. 407–432.

39 N. A. Ibrahim, U. Rashid, T. S. Y. Choong and I. A. Nehdi, *RSC Adv.*, 2020, **10**, 6098–6108.

40 K. Saravanan, B. Tyagi, R. S. Shukla and H. C. Bajaj, *Fuel*, 2016, **165**, 298–305.

41 M. Sarno and M. Iuliano, *Green Process. Synth.*, 2019, **8**, 828–836.